

Dear Editor Eleanor Browne and Referee,

Thanks for your suggestions which significantly help us to improve the manuscript. Hereby, we submit our responses and the manuscript has been revised accordingly. If there are any further questions or comments, please let us know.

Best regards

Guoxian Zhang on behalf of all co-authors

Key Lab. of Environmental Optics & Technology, Anhui Institute of Optics and Fine Mechanics, Chinese Academy of Sciences

230031 Hefei China

E-mail: [gxzhang@aiofm.ac.cn](mailto:gxzhang@aiofm.ac.cn)

## Major Comments

---

*1. Line 180: LIF groups now routinely use inlet-pre-injectors to chemically remove ambient OH prior to sampling (to determine their background signal for subtraction) to ensure an interference-free OH measurement. Wavelength modulation does not allow distinction between ambient OH and any OH internally generated within the reaction cell. A previous comparison exercise with a second LIF instrument at a different location does not ensure that the instrument (and the OH measurement presented here) is free from interferences. This needs to be acknowledged when discussing the model measurement comparison.*

### Reply:

Thanks for your suggestion. During the TROPSTECT-YRD campaign, we did not use an inlet-pre-injector to determine the chemical background of OH radical. We acknowledge your point that the comparison exercise with a second LIF instrument at a different location does not ensure that the instrument (and the OH measurement presented here) is free from interferences. We will discuss whether internal interference exists in AIOFM-LIF from the following aspects:

First of all, literature research shows that measurement interference is more related to the length of the inlet in the low-pressure cell (Griffith et al., 2016). In terms of system design, the AIOFM-LIF system uses a short-length inlet design to minimize this and other unknown disturbances (the distance from radical sampling to fluorescence excitation is ~150 mm).

Additionally, potential interference may exist when the atmosphere contains abundant alkenes, ozone, and BVOCs, indicating that environmental conditions play leading roles in OH interferences (Mao et al., 2010; Fuchs et al., 2016; Novelli et al., 2014). In the previous comparison exercise with a LIF instrument deployed an inlet pre-injector (PKU-LIF), the ozonolysis interference on the measurement consistency of both systems was excluded under high-VOCs conditions (Zhang et al., 2022).

We have compared the chemical conditions during the intercomparison

experiment and the current environmental conditions. Overall, the key parameters related to ozonolysis reactions ( $O_3$ , alkenes, isoprene and  $NO_x$ ) in TROPSTECT-YRD were similar to those during the comparison experiment, which is not conducive to generating potential OH interference.

**Table.** Comparison of key parameters related to ozonolysis reactions ( $O_3$ , alkenes, isoprene and  $NO_x$ ) between TROPSTECT-YRD and the intercomparison experiment. All the values are the diurnal average (10:00-15:00).

Species	Intercomparison	TROPSTECT-YRD
$O_3$ (ppb)	71.02	76.25
Alkenes (ppb)	1.29	0.67
Isoprene (ppb)	0.67	0.86
$NO_x$ (ppb)	5.65	6.55

To provide direct evidence on the OH chemical background signal, we conducted another atmospheric oxidation observation in the same location (Science Island background station in Hefei) and season (September, Autumn in 2022) in 2022, using chemical modulation methods to measure the chemical background of OH radicals in AIOFM-LIF instrument. The environmental conditions during ozone pollution (2022.9.29-2022.10.3) are shown in the Fig. S3, with daytime peaks of ozone concentration above 75 ppb, accompanied by alkene species approaching ~10 ppb. The diurnal concentration of isoprene was also a high level (>1 ppb). The chemical conditions are more favourable to induce OH interference than the TROPSTECT-YRD site. However, the OH concentrations achieved by chemical modulation ( $OH_{chem}$ ) and wavelength modulation ( $OH_{wav}$ ) were in good agreement. No obvious chemical background was observed by deploying an inlet pre-injector. Therefore, it is not expected that OH measurement in the present study was affected by internal interference.

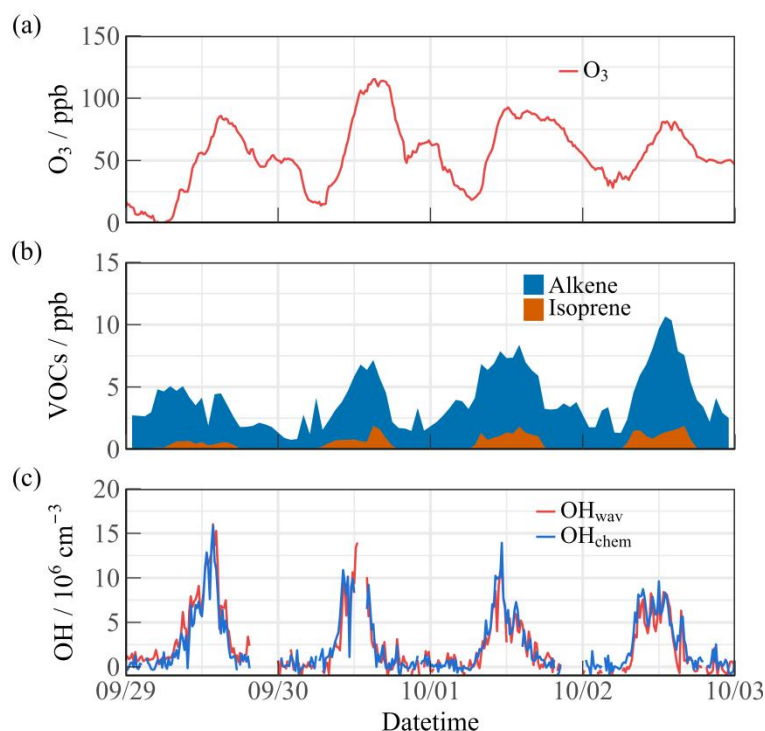


**Fig. S3.** Results of an additional atmospheric oxidation observation experiment in the same location and season in 2022. **(a)** Ozone concentration **(b)** Concentrations of alkene and isoprene, respectively. **(c)** The OH concentrations achieved by chemical modulation (OH<sub>chem</sub>) and wavelength modulation (OH<sub>wav</sub>).

We added the detailed description in Line 187-197.

### Revision:

**Line 187-197:** An additional atmospheric oxidation observation was conducted in the same location and season in 2022 with a chemical modulation method to determine the chemical background of OH radicals (Fig. S3). During the ozone pollution (2022.9.29-2022.10.3), the daytime peaks of ozone concentration above 75 ppb, accompanied by alkene species approaching ~10 ppb. The diurnal concentration of isoprene was also a high level (>1 ppb). The chemical conditions are more favourable to induce OH interference than in the TROPSTECT campaign, while the OH concentrations achieved by chemical modulation (OH<sub>chem</sub>) and wavelength modulation (OH<sub>wav</sub>) were in good agreement. No obvious chemical background was observed by deploying an inlet pre-injector. Therefore, it is not expected that OH measurement in the present study was affected by internal interference.

**2. Section 2.2.2: the description of the OH reactivity instrument lacks adequate detail. How is OH generated? Via the photolysis of ambient or generated ozone?**

*What was the initial OH concentration generated? Flow rate and pressure in the flow-tube?*

**Reply:**

Thank you for your reply. OH radicals are generated by laser photolysis of ambient ozone, using a laser pulse with a wavelength of 266 nm. Under conditions of 80 ppb O<sub>3</sub> and 8000 ppm water vapor concentration, the concentration of OH radicals produced in the flow tube remains at the order of 10<sup>9</sup> cm<sup>-3</sup>. The flow tube is at ambient pressure, with a gas flow rate of 17 SLM. We have supplemented the detailed description for the OH reactivity measurement instrument in Line 219-230.

**Revision:**

**Line 219-230:** The configuration structure for  $k_{\text{OH}}$  measurement has been detailed in a previous study(Liu et al., 2019). The flow tube in the OH production-reaction unit is at ambient pressure, with a gas flow rate of 17 SLM. A pulsed laser beam (266 nm with an average power of 15 mJ) is output from a frequency-quadrupled Nd:YAG laser, which generates stable OH radical through flash photolysis of ambient ozone in the flow tube. Consistent and stable production of OH radicals is ensured by maintaining a stable concentration of reactants, flow field, and laser energy. Under conditions of 80 ppb O<sub>3</sub> and 8000 ppm water vapor concentration, OH radicals produced in the flow tube remains at the concentration order of 10<sup>9</sup> cm<sup>-3</sup>. Subsequently, the OH radicals are sampled through a nozzle into a fluorescence cell. The OH fluorescence signal is then detected using laser pump and probe techniques and is fitted to calculate the slope of OH decay ( $k_{\text{OH}}$ ). The detection accuracy, achieved with an integration time of 180 s, is 0.3 s<sup>-1</sup> (1 $\sigma$ ).

**3. Section 2.3: A comprehensive list of model constraints should be provided.**

*Which NMHCs were measured?*

**Reply:**

Thank you for your reply. The comprehensive list of model constraints was provided in Table S3. The measured NMHCs include 29 alkanes, 11 alkenes, 15

aromatics, as well as acetylene and isoprene, and the specific names are also listed in Table S3. We have supplemented the detailed description in Line 237-239.

**Revision:**

**Line 237-239:** The comprehensive list of model constraints was provided in Table S3. The measured NMHCs include 29 alkanes, 11 alkenes, 15 aromatics, as well as acetylene and isoprene.

**Table.S3.** The comprehensive list of model constraints.

Categories	Species
Meteorology	Temperature, Relative humidity, Pressure, Jvalues
Trace gases	O <sub>3</sub> , NO, NO <sub>2</sub> , SO <sub>2</sub> , CO, PAN, HONO
Alkanes	methane, ethane, propane, n-butane, isobutane, cyclopentane, n-pentane, isopentane, cyclohexane, methyl cyclopentane, 2,3-dimethyl butane, 2,2-dimethyl butane, n-hexane, 2-methyl pentane, 3-methyl pentane, methyl cyclohexane, n-heptane, 2-methyl hexane, 2,3-dimethyl pentane, 2,4-dimethyl pentane, 3-methyl hexane, n-octane, 2,3,4-trimethyl pentane, 2-methyl heptane, 3-methyl heptane, 2,2,4-trimethyl pentane, n-nonane, n-decane, n-undecane, n-dodecane
Alkenes	ethene, propene, 1,3-butadiene, 1-butene, cis-2-butene, trans-2-butene, 1-pentene, cis-2-pentene, trans-2-pentene, 1-hexene, styrene
BVOCs	isoprene
Alkynes	acetylene
Aromatics	benzene, toluene, ethyl benzene, o-xylene, m-xylene, n-propyl benzene, isopropyl benzene, p-ethyl toluene, o-ethyl toluene, m-ethyl toluene, 1,2,4-trimethyl benzene, 1,3,5-trimethyl benzene, 1,2,3-trimethyl benzene, p-diethyl benzene, m-diethyl benzene
OVOCs	HCHO, acetaldehyde, MACR, MVK

**4. Line 223: Was the model unconstrained to O<sub>3</sub> and NO<sub>2</sub> in this scenario?**

**Reply:**

Thank you for your reply. In the base scenario, the species involved in Table S3 are constrained as boundary conditions. In the ozone-simulation mode that mentioned in Fig.S4, the model unconstrained to O<sub>3</sub> and NO on the basis of the base scenario. We summarized the sensitive test scenarios used in the manuscript in Table 1, and the detailed description in Line 237-239&241-247.

**Table.1.** The sensitive test scenarios utilized to improve the model-measurement consistency between OH, HO<sub>2</sub> and RO<sub>2</sub> radicals.

Scenario	Configuration	Purpose
----------	---------------	---------

Base	RACM2 updated with isoprene reaction scheme (LIM)	The base case with the species involved in Table S3 are constrained as boundary conditions.
X on	As the base scenario, but add the X mechanism, and the X level is between 0.25 - 0.5 ppb.	To untangle the missing OH source where base scenario failed.
MTS on	As the base scenario, but add a monoterpene source, and the monoterpene level is ~0.4 ppb.	Utilizing monoterpene-derived RO <sub>2</sub> to represent the alkoxy radicals with rather complex chemical structures.
MTS+X on	As the base scenario, but both the X mechanism and monoterpene source are considered.	To consider both the missing OH and RO <sub>2</sub> sources.
HAM on	As the base scenario, but add the reactive aldehyde chemistry.	To provide a test of whether the proposed mechanism can explain the missing OH source.
HAM on (4 × ALD)	As the base scenario, but add the reactive aldehyde chemistry, and the concentration of ALD was amplified by a factor of 4.	To quantify the impact of missing aldehyde primary emissions on RO <sub>x</sub> chemistry.
Ozone simulation	As the base scenario, but remove the constraints of the observed ozone and NO concentrations.	To test the suitable lifetime for the base model.
HCHO simulation	As the base scenario, but remove the constraint of the observed HCHO concentration.	To test the simulation effect of the existing mechanism on formaldehyde concentration.

### Revision:

**Line 237-239:** The comprehensive list of model constraints was provided in Table S3. The measured NMHCs include 29 alkanes, 11 alkenes, 15 aromatics, as well as acetylene and isoprene.

**Line 241-247:** An ozone-simulation test was conducted to determine the suitable atmospheric lifetime ( $\tau_D$ ) for the base model. At the lifetime of 24 hours, with a corresponding first-order loss rate of 1.1 cm/s (assuming a boundary layer height of 1 km), the simulated ozone concentration closely matched the observed values (Fig. S4). To improve the model-measurement consistency between OH, HO<sub>2</sub> and RO<sub>2</sub> radicals, a series of sensitivity analyses were performed to evaluate the impacts of potential mechanisms, as detailed in Table 1.

**5. Fig. 4 highlights that OVOCs contribute significantly to OH reactivity. Given that one of the major conclusions of the manuscript is that future measurement**

*campaigns should target more OVOCs, the individual OVOCs that are considered in this class should be provided. It would be beneficial to list all the VOCs that have been considered in all the different groups in a table. The calculated reactivity seems to compare well with the observed OH reactivity at the start of the measurement period, but then there is evidence of missing OH reactivity after the 10th, why is this? Was the contribution model-generated intermediates make to the calculated OH reactivity considered?*

**Reply:**

Thank you for your reply. We have listed the VOCs involved in the model simulation in Table S3 and have specifically detailed the contribution of OVOCs to OH reactivity (Fig. 4).

**Table.S3.** The comprehensive list of model constraints.

Categories	Species
Meteorology	Temperature, Relative humidity, Pressure, Jvalues
Trace gases	O <sub>3</sub> , NO, NO <sub>2</sub> , SO <sub>2</sub> , CO, PAN, HONO
Alkanes	methane, ethane, propane, n-butane, isobutane, cyclopentane, n-pentane, isopentane, cyclohexane, methyl cyclopentane, 2,3-dimethyl butane, 2,2-dimethyl butane, n-hexane, 2-methyl pentane, 3-methyl pentane, methyl cyclohexane, n-heptane, 2-methyl hexane, 2,3-dimethyl pentane, 2,4-dimethyl pentane, 3-methyl hexane, n-octane, 2,3,4-trimethyl pentane, 2-methyl heptane, 3-methyl heptane, 2,2,4-trimethyl pentane, n-nonane, n-decane, n-undecane, n-dodecane
Alkenes	ethene, propene, 1,3-butadiene, 1-butene, cis-2-butene, trans-2-butene, 1-pentene, cis-2-pentene, trans-2-pentene, 1-hexene, styrene
BVOCs	isoprene
Alkynes	acetylene
Aromatics	benzene, toluene, ethyl benzene, o-xylene, m-xylene, n-propyl benzene, isopropyl benzene, p-ethyl toluene, o-ethyl toluene, m-ethyl toluene, 1,2,4-trimethyl benzene, 1,3,5-trimethyl benzene, 1,2,3-trimethyl benzene, p-diethyl benzene, m-diethyl benzene
OVOCs	HCHO, acetaldehyde, MACR, MVK

In Fig. 4,  $k_{\text{OVOCs}}$  are categorized into three groups:  $k_{\text{OVOCs(Obs)}}$ ,  $k_{\text{OVOCs(Model)}}$ , and  $k_{\text{HCHO}}$ . Given the significance of formaldehyde photolysis, the contribution of HCHO to  $k_{\text{OVOCs}}$  is distinguished.  $k_{\text{OVOCs(Obs)}}$  encompasses species observed in addition to formaldehyde, such as acetaldehyde (ACD) and the oxidation products of isoprene

(MACR and MVK). Intermediates generated by the model, including glyoxal (GLY), methylglyoxal (MGLY), higher aldehydes (ALD), ketones (KET), methyl ethyl ketone (MEK), and methanol (MOH), are classified as  $k_{\text{OVOCs}(\text{Model})}$ . Upon considering  $k_{\text{OVOCs}(\text{Model})}$ , the calculated reactivity seems to compare well with the observed OH reactivity at the start of the measurement period, but then there is evidence of missing OH reactivity after September 10th (Fig.4(d)).

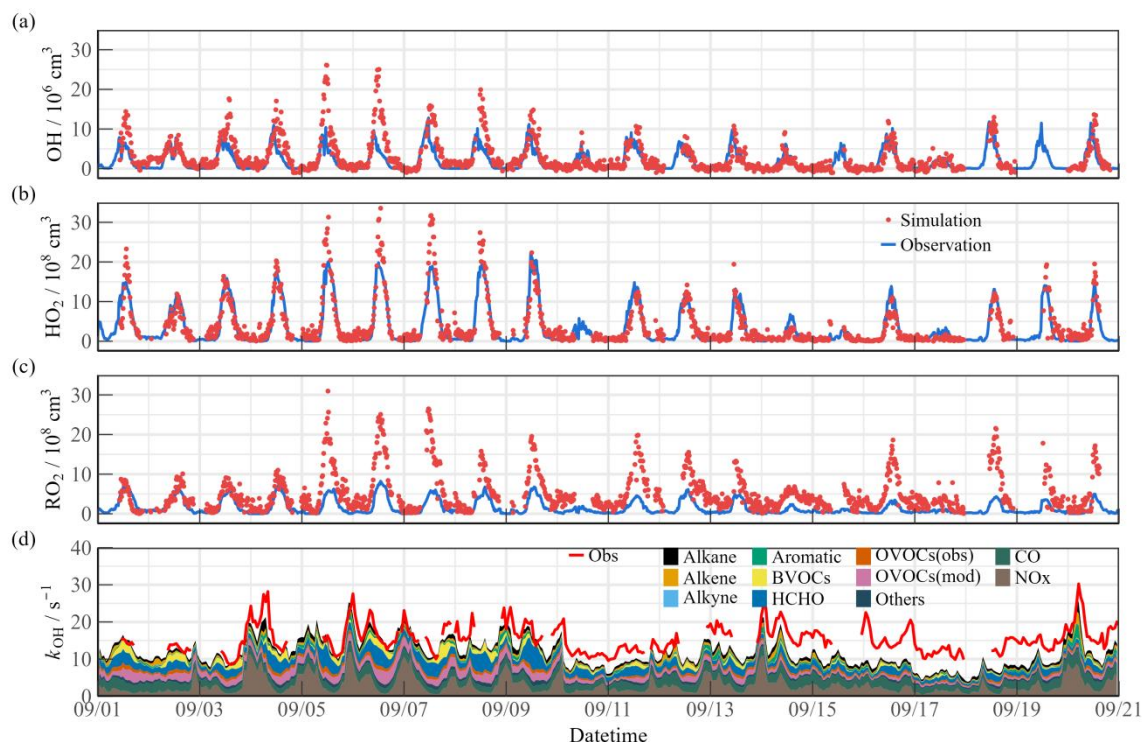


**Fig. 4.** Timeseries of the observed and modelled parameters for OH,  $\text{HO}_2$  and  $k_{\text{OH}}$  during the observation period. (a) OH, (b)  $\text{HO}_2$ , (c)  $k_{\text{OH}}$ .

Due to the limitations of available instruments, this observation only measured a limited number of OVOCs species, making it difficult to accurately quantify the contribution of larger aldehydes and ketones, carboxylic acids, nitrophenols, and other multifunctional species to  $k_{\text{OH}}$  (Wang et al., 2024). Since the MCM mechanism considers more secondary formation reactions than the RACM2 mechanism, it can qualitatively assess the photochemical role of unmeasured OVOCs species in the atmosphere (Wang et al., 2022b). The additional modeled OVOCs by the MCM v3.3.1 mechanism contributed  $\sim 2.4 \text{ s}^{-1}$  to the missing OH reactivity (Fig.S7). During Heavy period, the reactivity of more model oxidation products increased the daytime  $k_{\text{OH}}$  by about  $5.1 \text{ s}^{-1}$ . Therefore, the observed  $k_{\text{OH}}$  can serve as an upper limit for

sensitivity tests, thereby the full suite of radical measurement can be performed to explore the missing oxidation properties and ozone formation (Section 4.1).

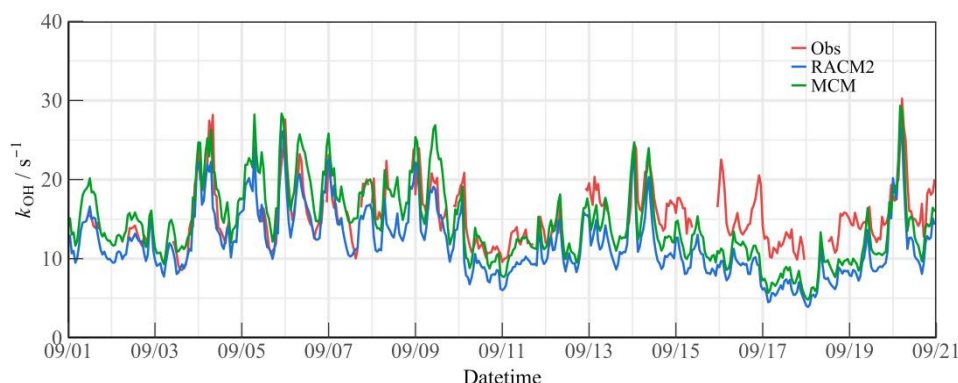


**Fig. S7.** Timeseries of the observed and modelled  $k_{OH}$  during the observation period.

We added the detailed description in Line 345-353&372-386.

### Revision:

**Line 345-353:**  $k_{OVOCs}$  are categorized into three groups:  $k_{OVOCs(Obs)}$ ,  $k_{OVOCs(Model)}$ , and  $k_{HCHO}$ . Given the significance of formaldehyde photolysis, the contribution of HCHO to  $k_{OVOCs}$  is distinguished.  $k_{OVOCs(Obs)}$  encompasses species observed in addition to formaldehyde, such as acetaldehyde (ACD) and the oxidation products of isoprene (MACR and MVK). Intermediates generated by the model, including glyoxal (GLY), methylglyoxal (MGLY), higher aldehydes (ALD), ketones (KET), methyl ethyl ketone (MEK), and methanol (MOH), are classified as  $k_{OVOCs(Model)}$ . Upon considering  $k_{OVOCs(Model)}$ , the reactivity calculated prior to September 10th aligns quite well with the observed OH reactivity.

**Line 372-386:** The calculated reactivity seems to compare well with the observed OH reactivity at the start of the measurement period, but then there is evidence of missing OH reactivity after September 10th (Fig. 4(d)). Due to the limitations of available instruments, this observation only measured a limited number of OVOCs species, making it difficult to accurately quantify the contribution of larger aldehydes and ketones, carboxylic acids, nitrophenols, and other multifunctional species to  $k_{OH}$  (Wang et al., 2024). Since the MCM mechanism considers more secondary formation reactions than the RACM2 mechanism, it can qualitatively assess the photochemical role of unmeasured OVOCs species in the atmosphere (Wang et al., 2022b). The additional modeled OVOCs by the MCM v3.3.1 mechanism contributed  $\sim 2.4 \text{ s}^{-1}$  to

the missing OH reactivity (Fig. S7). During Heavy period, the reactivity of more model oxidation products increased the daytime  $k_{OH}$  by about  $5.1 \text{ s}^{-1}$ . Therefore, the observed  $k_{OH}$  can serve as an upper limit for sensitivity tests, thereby the full suite of radical measurement can be performed to explore the missing oxidation properties and ozone formation (Section 4.1).

*6. Line 444-455: This section discusses the inclusion of monoterpenes in the model. The authors need to describe how RACM2 treats the oxidation of alpha-pinene and how this compares to the MCM mechanism for alpha pinene.*

**Reply:**

Thank you for your reply. The oxidation processes of  $\alpha$ -pinene and limonene related to RACM2 mechanism have been listed in Table S4, including the oxidation reactions with OH/O<sub>3</sub>/NO<sub>3</sub>, as well as the reactions of the derived alkoxy radicals (APIP) with NO/NO<sub>3</sub>/HO<sub>2</sub> and the self-reactions among peroxy radicals. In the MCM mechanism, the derivative of  $\alpha$ -Pinene, C96O2, could undergo four RO<sub>2</sub>→RO<sub>2</sub> propagations before returning to HO<sub>2</sub> radicals. An additional reaction was added to the base model in a previous research, converting OH into C96O2 (the oxidation product of  $\alpha$ -pinene) with a reaction rate equal to the missing reactivity, to explore the source of the missing RO<sub>2</sub> radicals(Whalley et al., 2021). In the RACM2 mechanism, the peroxy radicals generated from  $\alpha$ -pinene oxidation are classified as APIP and return to HO<sub>2</sub> radicals through subsequent reactions with NO. Therefore, we place greater emphasis on utilizing monoterpene-derived RO<sub>2</sub> in sensitive experiments to represent those RO<sub>2</sub> radicals with relatively complex chemical structures (Table 1).

**Table.S4.** Gas-phase kinetics for the monoterpene species in RACM2 mechanism. API and LIM stand for  $\alpha$ -pinene and limonene, respectively; APIP and LIMP represents peroxy radicals derived from API and LIM, respectively; ETHP refers to peroxy radicals generated from ethane; KETP denotes peroxy radicals formed from ketones; ALD signifies C<sub>3</sub> and higher aldehydes; KET indicates ketones; OLNN pertains to the NO<sub>3</sub>-alkene adduct that reacts to form carbonitrates and HO<sub>2</sub>; OLND pertains to the NO<sub>3</sub>-alkene adduct that reacts through decomposition; ACT signifies acetone; ORA1 denotes formic acid; ONIT represents organic nitrate; OP2 denotes higher organic peroxides; MO2 signifies methyl peroxy radical; MOH indicates methanol; ROH denotes C<sub>3</sub> and higher alcohols; ACO3 represents acetyl peroxy radicals; ORA2 denotes acetic acid and other higher acids.

Reaction	Reaction rate constant (cm <sup>3</sup> s <sup>-1</sup> )
API + OH → APIP	$1.21 \times 10^{-11} \exp(440/T)$
API + O <sub>3</sub> → 0.85 × OH + 0.1 × HO <sub>2</sub> + 0.2 × ETHP + 0.42 × KETP +	$5.0 \times 10^{-16} \exp(-530/T)$

$0.14 \times \text{CO} + 0.02 \times \text{H}_2\text{O}_2 + 0.65 \times \text{ALD} + 0.53 \times \text{KET}$	
$\text{API} + \text{NO}_3 \rightarrow 0.1 \times \text{OLNN} + 0.9 \times \text{OLND}$	$1.19 \times 10^{-12} \exp(490/T)$
$\text{APIP} + \text{NO} \rightarrow 0.82 \times \text{HO}_2 + 0.82 \times \text{NO}_2 + 0.23 \times \text{HCHO} + 0.43 \times \text{ALD} +$ $0.44 \times \text{KET} + 0.07 \times \text{ORA1} + 0.18 \times \text{ONIT}$	$4.0 \times 10^{-12}$
$\text{APIP} + \text{HO}_2 \rightarrow \text{OP2}$	$1.5 \times 10^{-11}$
$\text{APIP} + \text{MO}_2 \rightarrow \text{HO}_2 + 0.75 \times \text{HCHO} + 0.75 \times \text{ALD} + 0.75 \times \text{KET} +$ $0.25 \times \text{MOH} + 0.25 \times \text{ROH}$	$3.56 \times 10^{-14} \exp(708/T)$
$\text{APIP} + \text{ACO}_3 \rightarrow 0.5 \times \text{HO}_2 + 0.5 \times \text{MO}_2 + \text{ALD} + \text{KET} + \text{ORA2}$	$7.4 \times 10^{-13} \exp(765/T)$
$\text{APIP} + \text{NO}_3 \rightarrow \text{HO}_2 + \text{NO}_2 + \text{ALD} + \text{KET}$	$1.2 \times 10^{-12}$
$\text{LIM} + \text{OH} \rightarrow \text{LIMP}$	$4.2 \times 10^{-11} \exp(401/T)$
$\text{LIM} + \text{O}_3 \rightarrow 0.85 \times \text{HO} + 0.1 \times \text{HO}_2 + 0.16 \times \text{ETHP} + 0.42 \times \text{KETP} +$ $0.02 \times \text{H}_2\text{O}_2 + 0.14 \times \text{CO} + 0.46 \times \text{OLT} + 0.04 \times \text{HCHO} + 0.79 \times \text{MACR} +$ $0.01 \times \text{ORA1} + 0.07 \times \text{ORA2}$	$2.95 \times 10^{-15} \exp(-783/T)$
$\text{LIM} + \text{NO}_3 \rightarrow 0.71 \times \text{OLNN} + 0.29 \times \text{OLND}$	$1.22 \times 10^{-11}$
$\text{LIMP} + \text{NO} \rightarrow \text{HO}_2 + \text{NO}_2 + 0.05 \times \text{OLI} + 0.43 \times \text{HCHO} + 0.68 \times \text{UALD} +$ $0.07 \times \text{ORA1}$	$4.0 \times 10^{-12}$
$\text{LIMP} + \text{HO}_2 \rightarrow \text{OP}_2$	$1.5 \times 10^{-11}$
$\text{LIMP} + \text{MO}_2 \rightarrow \text{HO}_2 + 0.192 \times \text{OLI} + 1.04 \times \text{HCHO} + 0.308 \times \text{MACR} +$ $0.25 \times \text{MOH} + 0.25 \times \text{ROH}$	$3.56 \times 10^{-14} \exp(708/T)$
$\text{LIMP} + \text{ACO}_3 \rightarrow 0.5 \times \text{HO}_2 + 0.5 \times \text{MO}_2 + 0.192 \times \text{OLI} + 0.385 \times \text{HCHO} +$ $0.308 \times \text{MACR} + 0.5 \times \text{ORA2}$	$7.4 \times 10^{-13} \exp(765/T)$
$\text{LIMP} + \text{NO}_3 \rightarrow \text{HO}_2 + \text{NO}_2 + 0.385 \times \text{OLI} + 0.385 \times \text{HCHO} +$ $0.615 \times \text{MACR}$	$1.2 \times 10^{-12}$

---

Discrepancy of OH reactivity ( $\sim 3 - 5 \text{ s}^{-1}$ ) between measurement and model suggested that an additional driving force was necessary to complete the OH to RO<sub>2</sub> step. In the TROPSPECT campaign, approximately 0.4 ppb of monoterpene was introduced into the base scenario as the chemical reactions of complex alkoxy radicals, which is similar to an atmospheric level in the EXPLORE-2018 campaign, the YRD region (Wang et al., 2022a). Sensitivity tests were conducted by incorporating API and LIM into the 'MTS on' and 'MTS+X on' scenarios as the chemical reactions of complex alkoxy radicals, respectively (Ma et al., 2022). We added the detailed description in Line 535-555.

### Revision:

**Line 535-555:** The union of  $k_{\text{OH}}$  and RO<sub>2</sub> measurement can help reveal the magnitude of missing RO<sub>2</sub> as a hypothesis of sensitivity analysis. An additional reaction was added to the base model in a previous research, converting OH into C<sub>9</sub>H<sub>16</sub>O<sub>2</sub> (the oxidation product of  $\alpha$ -pinene) with a reaction rate equal to the missing reactivity, to explore the source of the missing RO<sub>2</sub> radicals (Whalley et al., 2021). Discrepancy of OH reactivity ( $\sim 3 - 5 \text{ s}^{-1}$ ) between measurement and model suggested that an

additional driving force was necessary to complete the OH to RO<sub>2</sub> step. In the TROPSPECT campaign, approximately 0.4 ppb of monoterpene was introduced into the base scenario as the chemical reactions of complex alkoxy radicals, which is similar to an atmospheric level in the EXPLORE-2018 campaign, the YRD region (Wang et al., 2022a). The RACM2 mechanism identified  $\alpha$ -pinene (API) and limonene (LIM) as representative monoterpenes species. Sensitivity tests were conducted by incorporating API and LIM into the 'MTS on' and 'MTS+X on' scenarios, respectively (Ma et al., 2022). The mean of these values was considered the average effect of monoterpenes chemistry, and depicted as the green line in Fig. 6. In the 'MTS on' scenario, the chemistry of peroxy radicals in Semi II was reasonably described by introducing the source of complex alkoxy radicals, and the obs-to-mod ratio of peroxy radicals decreased from 2.2 to 1.3. Furthermore, the introduction of additional complex alkoxy radicals had minimal impact on HO<sub>x</sub> chemistry, with changes in daytime OH and HO<sub>2</sub> concentrations of less than  $5 \times 10^5 \text{ cm}^{-3}$  and  $2.5 \times 10^7 \text{ cm}^{-3}$ , respectively. This demonstrates the robustness of HO<sub>x</sub> radical in response to potential monoterpene.

*7. Section 4.3: I found this section particularly difficult to follow. What do the authors mean by 'Special HCHO' ? Could the authors provide the model predicted HCHO concentration (when left unconstrained to HCHO) relative to the HCHO concentration measured? The main conclusion of this section seems to be that other OVOC (that can act as a source of RO<sub>2</sub>) should be measured, but there is no discussion on what OVOCs were measured beyond HCHO; this detail needs to be included.*

**Reply:**

Thank you for your response. The term "special HCHO" mentioned in the manuscript aims to emphasize a phenomenon where formaldehyde has a high concentration distribution (with an average concentration of  $21.81 \pm 4.57$  ppb at noon), but the contributions of OVOCs to the RO<sub>x</sub> radical do not exhibit the same intensity as formaldehyde, and the current mechanism encounters difficulties in replicating

formaldehyde concentrations. We acknowledge your point that this part of the description is too confusing. Therefore, we have changed the title of the relevant section to "4.3 Missing OVOCs sources influence ozone production" and adjusted the content of that section. We have removed the impact of formaldehyde on the length of the reaction chain and its oxidizing effect, focusing more on the diagnostic of the HO<sub>2</sub>/RO<sub>2</sub> ratio on ozone formation to improve the readability of the manuscript.

The information on the measured OVOCs species has been integrated into Supplementary Table S3, and their contributions to  $k_{OH}$  are discussed in detail on Lines 372-386 and in Supplementary Fig.S7. The comparison results between the simulated and measured values of formaldehyde concentrations are shown in the Fig. S11. The deposition time is set to 24 hours, and a comparative analysis has been conducted based on the MCM v3.3.1 mechanism and RACM2-LIM1 mechanism. The results show that the simulated formaldehyde concentrations are significantly lower than the observation. In addition to possible missing primary source emission data, the existence of currently undiscovered VOCs cannot be ruled out, which may act as a secondary source of formaldehyde through multiple RO<sub>2</sub> + NO reaction steps (Färber et al., 2024).

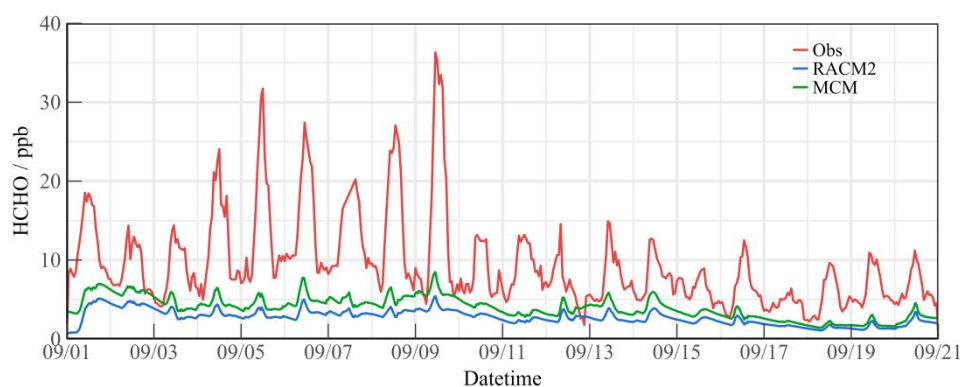


**Fig. S11.** The observed and modeled HCHO concentration during the TROPSTECT-YRD campaign.

We also analyzed the impact of the missing OVOCs sources on RO<sub>2</sub> radicals and ozone production. When formaldehyde levels are unconstrained, the simulated HO<sub>2</sub>/RO<sub>2</sub> ratios align with observations, suggesting that under the prevailing chemical mechanism, the photochemical efficiency of formaldehyde and other OVOCs is similar. Therefore, an empirical hypothesis is proposed to amplify the concentration

of higher-order aldehydes by a factor of about 4, which is the proportion of formaldehyde concentration underestimated by the model. The qualitative assessment of the impact of missing aldehyde primary emissions on RO<sub>2</sub> radical concentrations was combined with the HAM mechanism across the entire photochemical spectrum (Fig.S12). Enhanced impact of aldehyde autoxidation in the presence of weak photochemical conditions could alter the simulated levels of OH and HO<sub>2</sub> radicals by approximately 13.9% and 18.1%, respectively. However, higher ALD concentrations will be achieved under intensive photochemical conditions, leading to the gradual dominance of the sink channels for OH + OVOCs, with the effect of autoxidation mechanisms gradually decreasing. RO<sub>2</sub> radical concentrations is notably more sensitive to the HAM mechanism, where incorporates additional OVOCs, can enhance the simulation of RO<sub>2</sub> radical concentrations by 20 - 40%.

We added the detailed description in Line 661-712.

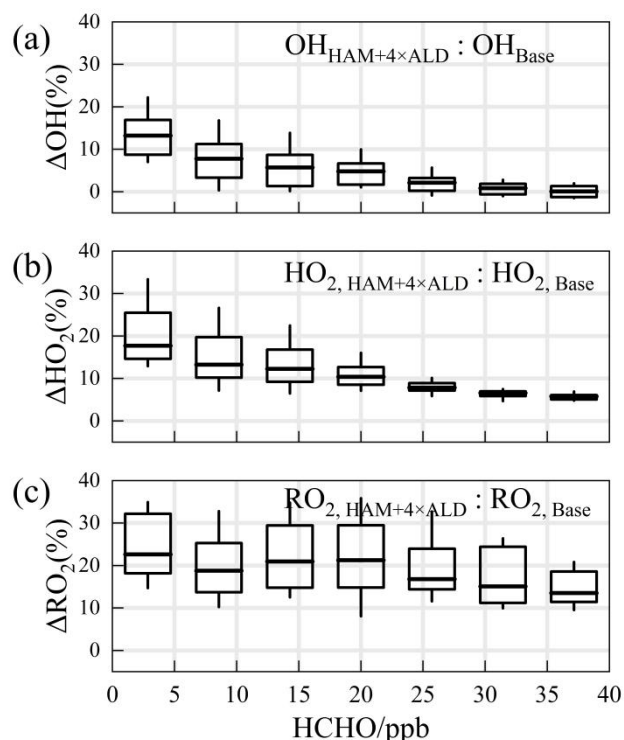


**Fig. S12.** The relationship between the differences in the simulation of (a) OH, (b) HO<sub>2</sub>, and (c) RO<sub>2</sub> radical concentrations by HAM mechanism and the base scenario across the entire photochemical spectrum. An empirical hypothesis is proposed to amplify the concentration of higher-order aldehydes by a factor of about 4, which is the proportion of formaldehyde concentration underestimated by the model. The boxplots represent the 10%, 25%, median, 75%, and 90% of the data, respectively.

**Revision:**

**Line 660:** 4.3 Missing OVOCs sources influence ozone production

**Line 661-712:** The consistency between model predictions and observed measurements for ozone production, akin to the concentration ratio of  $\text{HO}_2/\text{RO}_2$ , is depicted in Fig. 11(a)(b). In areas with low NO levels, the ratio of modeled to actual ozone production ranges from 0.5 to 2, with the exception of the ClearfLo and AIRPRO-summer datasets (Woodward-Massey et al., 2023; Whalley et al., 2021). Conversely, under high NO conditions (with NO concentrations between 3 and 6 ppbv), the ozone production rate ( $\text{P}(\text{Ox})$ ) derived from measured radical concentrations typically exceeds that of the base model's predictions by more than threefold. Laboratory experiments focusing on the oxidation of representative VOCs suggest that ozone production can be enhanced by approximately 25% for the anthropogenic VOCs under investigation (Färber et al., 2024). The MTS+X scenario represents an effort to enhance the congruence between modeled and measured radical concentrations. The incorporation of OVOCs and larger alkoxy radicals derived from monoterpenes has refined the model-measurement agreement for ozone formation under high NO conditions, reducing the discrepancy from 4.17 to 2.33. This substantiates the hypothesis of sensitivity analysis concerning ozone generation, as detailed in Section 4.2 and illustrated in Fig. S10.

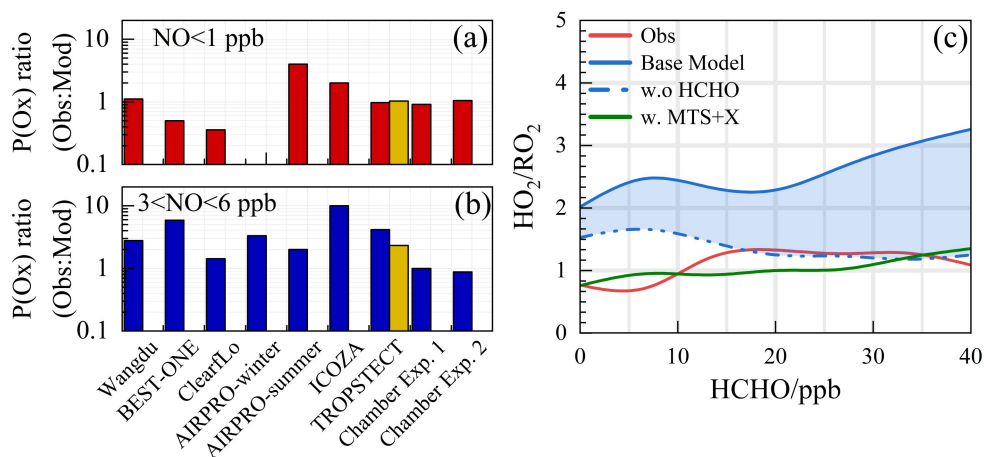


**Fig. 11.** Summary of the  $\text{P}(\text{Ox})_{\text{Obs}}/\text{P}(\text{Ox})_{\text{Mod}}$  under (a) low-NO and (b) high-NO conditions. (c) The ratios for  $\text{HO}_2/\text{RO}_2$  show a correlation with HCHO levels. The blue shading represents the range of variation from constrained to unconstrained formaldehyde conditions. Chamber Exp. 1 and Chamber Exp. 2 denotes the parameters by single-step  $\text{HO}_2$  formation and multi-step  $\text{HO}_2$  formation determined in the chamber by (Färber et al., 2024).

The reasons for the discrepancy between simulated and observed values for

ozone production deserve further investigation. As depicted in Fig.11(c), the simulated HO<sub>2</sub>/RO<sub>2</sub> ratios display a robust positive correlation with photochemical activity, fluctuating between 2 and 4. A notable feature during severe ozone pollution is the intense distribution of formaldehyde, with an average concentration of 21.81 ± 4.57 ppb (11:00 – 13:00). While formaldehyde acts as a precursor for HO<sub>2</sub> radicals, it does not directly generate RO<sub>2</sub> radicals. The contributions of OVOCs to the RO<sub>x</sub> radical do not exhibit the same intensity as formaldehyde, and the current mechanism encounters difficulties in replicating formaldehyde concentrations (Fig. S11). The simulation of formaldehyde concentrations using the MCM v3.3.1 mechanism has shown improvement, indicating that the secondary formation of unmeasured species, such as OVOCs, will feedback on RO<sub>2</sub> radical levels. When formaldehyde levels are unconstrained, the simulated HO<sub>2</sub>/RO<sub>2</sub> ratios align with observations, suggesting that under the prevailing chemical mechanism, the photochemical efficiency of formaldehyde and other OVOCs is similar. Therefore, an empirical hypothesis is proposed to amplify the concentration of higher-order aldehydes by a factor of about 4, which is the proportion of formaldehyde concentration underestimated by the model. The qualitative assessment of the impact of missing aldehyde primary emissions on RO<sub>2</sub> radical concentrations was combined with the HAM mechanism across the entire photochemical spectrum (Fig.S12). Enhanced impact of aldehyde autoxidation in the presence of weak photochemical conditions could alter the simulated levels of OH and HO<sub>2</sub> radicals by approximately 13.9% and 18.1%, respectively. However, higher ALD concentrations will be achieved under intensive photochemical conditions, leading to the gradual dominance of the sink channels for OH + OVOCs, with the effect of autoxidation mechanisms gradually decreasing. RO<sub>2</sub> radical concentrations is notably more sensitive to the HAM mechanism, where incorporates additional OVOCs, can enhance the simulation of RO<sub>2</sub> radical concentrations by 20 - 40%. Consequently, although limiting formaldehyde can partially offset the HO<sub>2</sub> radical cycle and enhance the precision of HO<sub>x</sub> radical chemistry studies, additional measurements should be undertaken for other OVOCs, coupled with the deployment of full-chain radical detection systems, to accurately elucidate the oxidation processes

under severe ozone pollution conditions.

## Minor Comments

---

*1. Line 38: Define 'ChL'*

**Reply:**

The relevant deception in the abstract has been deleted.

*2. Line 232 and 235: the different notations used in (2) and (3) need to be defined.*

**Reply:**

The relevant modifications have been added to Line 264-265.

**Revision:**

**Line 264-265:** Here, the OH yields from ozone photolysis and ozonolysis reactions are denoted as  $\varphi_{OH}$  and  $\varphi_{OH}^i$ , respectively.

## References

- Färber, M., Fuchs, H., Bohn, B., Carlsson, P. T. M., Gkatzelis, G. I., Marcillo Lara, A. C., Rohrer, F., Vereecken, L., Wedel, S., Wahner, A., and Novelli, A.: Effect of the Alkoxy Radical Chemistry on the Ozone Formation from Anthropogenic Organic Compounds Investigated in Chamber Experiments, *ACS ES&T Air*, 1, 1096-1111, 10.1021/acsestair.4c00064, 2024.
- Fuchs, H., Tan, Z., Hofzumahaus, A., Broch, S., Dorn, H.-P., Holland, F., Kuenstler, C., Gomm, S., Rohrer, F., Schrade, S., Tillmann, R., and Wahner, A.: Investigation of potential interferences in the detection of atmospheric ROx radicals by laser-induced fluorescence under dark conditions, *Atmos Meas Tech*, 9, 1431-1447, 10.5194/amt-9-1431-2016, 2016.
- Griffith, S. M., Hansen, R. F., Dusanter, S., Michoud, V., Gilman, J. B., Kuster, W. C., Veres, P. R., Graus, M., de Gouw, J. A., Roberts, J., Young, C., Washenfelder, R., Brown, S. S., Thalman, R., Waxman, E., Volkamer, R., Tsai, C., Stutz, J., Flynn, J. H., Grossberg, N., Lefer, B., Alvarez, S. L., Rappenglueck, B., Mielke, L. H., Osthoff, H. D., and Stevens, P. S.: Measurements of hydroxyl and hydroperoxy radicals during CalNex-LA: Model comparisons and radical budgets, *J Geophys Res-Atmos*, 121, 4211-4232, 10.1002/2015jd024358, 2016.
- Liu, S., Li, X., Shen, X., Zeng, L., Huang, X., Zhu, B., Lin, L., and Lou, S.: Measurement and partition analysis of atmospheric OH reactivity in autumn in Shenzhen, *Acta Scientiae Circumstantiae*, 39, 3600-3610, 2019.
- Ma, X., Tan, Z., Lu, K., Yang, X., Chen, X., Wang, H., Chen, S., Fang, X., Li, S., Li, X., Liu, J., Liu, Y., Lou, S., Qiu, W., Wang, H., Zeng, L., and Zhang, Y.: OH and HO<sub>2</sub> radical chemistry at a suburban site during the EXPLORE-YRD campaign in 2018, *Atmos Chem Phys*, 22, 7005-7028, 10.5194/acp-22-7005-2022, 2022.
- Mao, J., Ren, X., Chen, S., Brune, W. H., Chen, Z., Martinez, M., Harder, H., Lefer, B., Rappenglück, B., Flynn, J., and Leuchner, M.: Atmospheric oxidation capacity in the summer of Houston 2006: Comparison with summer measurements in other metropolitan studies, *Atmos Environ*, 44, 4107-4115, 10.1016/j.atmosenv.2009.01.013, 2010.
- Novelli, A., Hens, K., Ernest, C. T., Kubistin, D., Regelin, E., Elste, T., Plass-Duelmer, C., Martinez, M., Lelieveld, J., and Harder, H.: Characterisation of an inlet pre-injector laser-induced fluorescence instrument for the measurement of atmospheric hydroxyl radicals, *Atmos Meas Tech*, 7, 3413-3430, 10.5194/amt-7-3413-2014, 2014.
- Wang, H., Ma, X., Tan, Z., Wang, H., Chen, X., Chen, S., Gao, Y., Liu, Y., Liu, Y., Yang, X., Yuan, B., Zeng, L., Huang, C., Lu, K., and Zhang, Y.: Anthropogenic monoterpenes aggravating ozone pollution, *Natl. Sci. Rev.*, 9, 2022a.
- Wang, W., Yuan, B., Su, H., Cheng, Y., Qi, J., Wang, S., Song, W., Wang, X., Xue, C., Ma, C., Bao, F., Wang, H., Lou, S., and Shao, M.: A large role of missing volatile organic compound reactivity from anthropogenic emissions in ozone pollution regulation, *Atmos Chem Phys*, 24, 4017-4027, 10.5194/acp-24-4017-2024, 2024.
- Wang, W., Yuan, B., Peng, Y., Su, H., Cheng, Y., Yang, S., Wu, C., Qi, J., Bao, F., Huangfu, Y., Wang, C., Ye, C., Wang, Z., Wang, B., Wang, X., Song, W., Hu, W., Cheng, P., Zhu, M., Zheng, J., and Shao, M.: Direct observations indicate photodegradable oxygenated volatile organic compounds (OVOCs) as larger contributors to radicals and ozone production in the atmosphere, *Atmos Chem Phys*, 22, 4117-4128, 10.5194/acp-22-4117-2022, 2022b.

Whalley, L. K., Slater, E. J., Woodward-Massey, R., Ye, C., Lee, J. D., Squires, F., Hopkins, J. R., Dunmore, R. E., Shaw, M., Hamilton, J. F., Lewis, A. C., Mehra, A., Worrall, S. D., Bacak, A., Bannan, T. J., Coe, H., Percival, C. J., Ouyang, B., Jones, R. L., Crilley, L. R., Kramer, L. J., Bloss, W. J., Vu, T., Kotthaus, S., Grimmond, S., Sun, Y., Xu, W., Yue, S., Ren, L., Acton, W. J. F., Hewitt, C. N., Wang, X., Fu, P., and Heard, D. E.: Evaluating the sensitivity of radical chemistry and ozone formation to ambient VOCs and NO<sub>x</sub> in Beijing, *Atmos Chem Phys*, 21, 2125-2147, 10.5194/acp-21-2125-2021, 2021.

Woodward-Massey, R., Sommariva, R., Whalley, L. K., Cryer, D. R., Ingham, T., Bloss, W. J., Ball, S. M., Cox, S., Lee, J. D., Reed, C. P., Crilley, L. R., Kramer, L. J., Bandy, B. J., Forster, G. L., Reeves, C. E., Monks, P. S., and Heard, D. E.: Radical chemistry and ozone production at a UK coastal receptor site, *Atmos Chem Phys*, 23, 14393-14424, 10.5194/acp-23-14393-2023, 2023.

Zhang, G., Hu, R., Xie, P., Lu, K., Lou, S., Liu, X., Li, X., Wang, F., Wang, Y., Yang, X., Cai, H., Wang, Y., and Liu, W.: Intercomparison of OH radical measurement in a complex atmosphere in Chengdu, China, *Sci Total Environ*, 155924, 10.1016/j.scitotenv.2022.155924, 2022.